Supplementary information

Phosphine gas in the cloud decks of Venus

In the format provided by the
authors and unedited

Supplementary Information;

Phosphine Gas in the Cloud Decks of Venus

Astronomical observations

Details of the JCMT data acquisition and reduction approach

The James Clerk Maxwell Telescope is a 15m dish on Mauna Kea, Hawaii. All JCMT observations are available in the public archive at CADC, under project id S16BP007 (a Service Programme approved in semester 2016B), and were made with the RxA3 receiver and the ACSIS correlator. Full details are listed here to facilitate independent analysis of the raw data.

The earliest observations only established the best sideband tuning and the additional length of time needed in calibration (to avoid correlated noise from the bright planetary signal). The usable observations were taken on mornings of June 2017: the 9th (observation #49), 11th (#96,97), 12th (#97,100), 14th (#76,78) and 16th (#49,52,55,59). Each observation had 14 samples of ~2 min duration dumped by ACSIS (except that #97,100 on 12th June comprise one standard observation split into two parts). Hence the total number of independent spectra obtained is 140. The ACSIS setup provided 8192 spectral channels across a 250 MHz passband, resulting in channel-widths equivalent to 0.03427 km/s.

One other observation (#79 on 10th June) has been rejected from the analysis as it was excessively noisy, possibly due to an accidental short calibration. A number of shorter observations also appear in the archive, that were terminated by the telescope operator due to a receiver lost-lock report. Some of these were possibly false alarms, but we rejected all these short observations, which would add only 10% to the total time spent observing Venus.

At the time of observation, Venus was just over half-illuminated (phase of 0.55) and subtended 22 arcseconds. Hence the limb is downweighted by ~50%, given the approximately 19 arcsec full-width half-maximum of the telescope beam. The observations were made by beam-switching (chopping the telescope's secondary mirror) off Venus by 60 arcsec to remove the terrestrial sky signal. All ten observations over the five observing days are comparable in quality, with mean and standard deviation in system temperature of 460 K and 50 K respectively. The sky opacities at 225 GHz ranged from 0.09 to 0.17 (from simultanous JCMT Water Vapor Radiometer data) and the airmasses towards Venus ranged from 1.01 to 1.90. Data were taken at UT from 15:30 to 20:40 (observation mid-points), corresponding to 05:30 to 10:40 in local (Hawaii) time.

The observations started later than intended (in semester 2017A), as they were delayed by the calibration procedure being established. As a result, Venus' recession from the Earth caused it to underfill the telescope beam, and the continuum signal (expressed in antenna temperature units, T_A^*) is less than the brightness temperature of Venus at 266.9445 GHz. The mean continuum signal over the observations was $T_A^* = 152$ K, with standard deviation of 15 K. The continuum strength also varied significantly between some sub-observations, even though only ~2 min apart, probably due to imperfect telescope tracking. This could reduce sensitivity but has no effect in our line analysis, as a line-to-continuum (l:c) spectrum was created for each sub-observation.

Two dominant sources of spectral wave-effects (ripples) exist. The primary wave may be from reflection between the main dewar and cold-load dewer (distance ~0.5 m) and the secondary

wave from an unidentified surface near the middle of the receiver cabin (of diameter a little over 3 m), with these distances derived from a relation in ref. 43. The dominant ripple is quasi-sinusoidal, with amplitude up to ±2 Kelvin in antenna-temperature T_A^*. This was fitted with a 4th-order polynomial across the passband (better matching the data than a pure sine function). After subtracting this component, a second much fainter quasi-sinusoid was then removed. Because of its low amplitude (up to ~0.1 K, comparable to possible line strengths), this step was implemented by average-filtering the spectrum over a moving-box of 1024 channels, fitting a 9th-order polynomial to the filtered spectrum, and then subtracting this polynomial from the unfiltered data.

After subtraction of these components, a third residual ripple remains. By Fourier analysis of the 2-D dataset (time versus spectral channel; Supplementary Figure 1), this third component has periods that cluster around 8 and 16 waves fitting across the passband. These "2^n waves" can result when signal spikes have been processed during correlation. However, at the JCMT there is a known "16 MHz ripple" from reflection between the receiver and the secondary mirror unit, and/or due to cables between the receiver cabin and Nasmyth switch. Since 16 periods of 16 MHz would occupy 256 MHz, and the correlator was configured for a 250 MHz band, these reflections are likely the cause of the 16-period ripple we see (with the 8-period features probably being a modulation).

In principle, the whole 2-D dataset could be collapsed down on the time axis, and then a single polynomial could be fitted to remove the spectral ripple. The data were independently reduced in this way by one of the co-authors, and the phosphine line was recovered. However, we chose the three-step method as optimum for signal-to-noise, relation to physical effects, and ability to generate per-channel noise and check for any peculiar sub-observations (none were identified).

Fourier transform analysis was additionally performed, within KAPPA. There appears to be insufficient signal-to-noise that an FT could capture the phase-drifts shown in Supplementary Figure 1, and so we could not remove the ripples in Fourier space. In particular, the amplitudes of the main FT components were only about half those amplitudes seen in a median filter of the data. The observations have up to six significant features in Fourier space (defined as peaks > 5σ in the Hermitian-transform image), which results in ripple features not repeating within the passband. This also prevented us from using a fitting method based on a ripple 'template', i.e. a known baseline structure established away from Venus' velocity, that could be applied to the region covering the phosphine line.

The removal of the line wings in the reduction means that the line-center l:c value somewhat under-estimates the true line depth. We processed our model line in the same way as the data (Figure 1b), fitting an 8th-order polynomial outside the specified line region. This approach is difficult to perform fully realistically, as the ripple artefacts do not repeat within the passband, and so we could not inject such systematics appropriate to the Venus velocity into the model. Some additional tests were made combining our model line with noise plus sine-wave ripples of appropriate periods, and for |v| = 8 km/s the line-minimum is then seen at ~60% of its true value. However, there is significant dispersion, with e.g. a few percent of cases recovering the full line depth, in 1000 tests with different seeds for the random sine waves. In the main text, we adopt the simpler method of processing the noiseless model in our adopted |v| = 5 km/s case, which has also resulted in l:c of ~60% of the original model depth. Our 20 ppb solution after this processing (Figure 1b) fits the observed spectrum well in both line depth and width.

Details of the ALMA data acquisition and reduction approach

The Atacama Large Millimetre/submillimetre Array (ALMA) is located on a high plateau site in Chile. A total of forty-four 12m antennas were used, giving baselines of 15-314 m in a compact configuration of ALMA. Our data were obtained under Director's Discretionary Time, as project 2018.A.00023.S. Venus was observed on 2019 March 5 in two contiguous execution blocks (EBs) between 12:19 and 15:50 UTC (between 08:19 and 11:50 in Chilean Standard Time). Compared to the JCMT observation, Venus was somewhat more distant when viewed with ALMA (subtending 15 arcsec) and was also consequently more illuminated (phase of 0.74). Callisto was observed as the bandpass and flux-scale calibrator and J2000-1748 as the phase reference source. System temperatures in the spectral windows (spw) covering the line were around 100 K (between 80-160 K depending on antenna) with no telluric features in the high-resolution spw (the nearest being located at 267.3 GHz). Sky temperatures were 31-34 K in the direction of Venus, and receiver temperatures were 46-51 K. Atmospheric transmission in the high-resolution spw was in the range 89-91%, and precipitable water vapour (PWV) was 1.6 to 2.1 mm, at the lower range of the standard conditions for observing in ALMA Band 6.

We used four frequency bands in two pairs; one of each pair of width 1.875 GHz and the other of 0.1171875 GHz, each divided into 1920 spectral channels. One pair was centred on ~266.9 GHz and the other on ~266.1 GHz. The exact frequency was set at the start of each block to rest frequencies of 266.944662 and 266.16107 GHz, corrected for the motion of Venus. These are the rest frequencies of our PH_3 and HDO transitions (but noting that we updated the PH_3 rest-frequency in data-analysis, see below). In order to minimise instrumental effects, each frequency band was observed with three different combinations of local oscillator settings (as recommended by ALMA staff), resulting in three spectral windows (spw) for the same final frequency width and resolution. This mitigates the effect of the brightness of Venus on the bandpass dyamic range. We then reduced the effects of stochastic noise by averaging by approximately 8 channels to achieve the velocity resolution of 0.55 km s-1 used in analysis, and reduced the effects of residual ripples by baseline fitting after the extraction of spectra, as described in Methods.

Standard bandpass calibration could not remove ripples due to the large angular size of Venus being poorly sampled by the shortest baselines and to polarization-dependent primary beam effects, apparent for a planet of a few-thousand Jansky (Jy). These ripples were dependent on baseline length, not antenna. After experimenting with flagging baselines <20 to <50 m, and selective flagging of specific baselines, we found that excluding baselines <33 m gave a balance between the amount of ripple produced by shorter baselines and the increase in noise due to removing baselines becoming greater than the residual ripple amplitude. This means that the largest angular scale (LAS) imaged reliably (detected) is 4.3 (7.1) arcsec. According to the current ALMA definition of LAS, the baselines >33m correspond to 5.6 arcsec but imaging will be less reliable close to this scale for narrow spectral channels.

In all calibrations, we inserted the 'Butler-JPL-Horizons 2012' model for Venus. The phase scatter of the calibrated phase reference data is ~5 degrees. Each phase reference scan is ~25 sec. Venus was phase-only self-calibrated (excluding the central channels where the line is expected) using a 30s solution interval. The Venus phase solutions have a similar scatter although the corrected phases are dominated by the structure of Venus. The diameter of Venus produces at

least 17 nulls in our uv range, so there was insufficient signal-to-noise for amplitude self-calibration of all antennas, despite hundreds-of-Jy fluxes on the shortest baselines.

Using baselines longer than 33 m, the synthesised beam was 1.088 × 0.777 arcsec, at position angle PA = -88.5°. The image used for analysis was made (see Supplementary Software 4) with a spectral resolution of 0.55 km/s, to reduce the effects of stochastic noise and to match binned JCMT spectra. The ALMA rms near the field-centre is ~3.5 mJy/beam per channel. In all cases, the primary beam correction is applied; the edge of Venus corresponds to about 70% sensitivity.

ALMA data analysis: additional checks

In case artificial lines could be produced by applying too high an order in polynomial-fitting, we repeated the data-processing steps of self-calibration and continuum subtraction, but instead of excluding the 400 channels around the band centre, where the line was expected, we performed two alternative reductions excluding 400 channels below and above this central spectral region. We then imaged these channels and analysed them to produce whole-planet spectra, and the outputs are shown in Supplementary Figure 4. The l:c line-integrated signals are 14-22% of the value for the real line, and only ~2 channels in each case appear significant, i.e. the artefacts are narrow. Lorentzian fits to these artefacts give FWHM only half that of the real line (1.8, 2.4 km/s versus 4.1 km/s). This test shows that polynomial fitting does *not* artificially produce features that have profiles like the real PH_3 line predicted by realistic radiative transfer models of the atmosphere. To check the robustness of the PH_3 line centroid velocities (Table 1), we also used as an alternative 1st-order polynomial (linear fits) connecting spectral sections spanning ~5 km/s immediately adjacent to each side of the absorption feature, and then calculated centroids over ±3 km/s ranges. The wideband data provide a consistent but lower-quality estimate of the centroid. These data also in principle include the line wings, but these are obscured by ripple.

All ALMA l:c values have been derived using continuum flux densities of the relevant regions on the planet. These fluxes were measured separately from a continuum data product (imaged with all baselines). This aspect differs from the JCMT products, where each sub-observation contains its own continuum signal. The respective ALMA continuum fluxes are 16.1 (whole planet), 16.3 (equatorial zone), 16.2 (mid-latitudes) and 13.8 (polar caps) Jy/beam. Standard deviations are ~0.1-0.2 Jy/beam, so the fluxes averaged across these areas will more precise than this. No flux differences between northern and southern hemispheres were identified at this precision, but there may be small longitudinal variations (hence possibly with Sun-angle) at ~±0.1 Jy/beam levels.

The continuum image has good fidelity (for example, demonstrating some expected cooling at the poles), and has a whole-planet primary-beam-corrected flux of 2769 Jy at 266.9 GHz. This is 110% of the flux of 2508 Jy on the observing date estimated in the online SMA planetary visibility tool. This difference is moderate given uncertainties in absolute flux calibration, e.g. from the atmospheric temperature assumed in VIRA, and from ~5-7% uncertainty in transferring the flux scale from Callisto. However, the (narrowband) line-fluxes are significantly reduced by the omission of baselines of length <33 m, a reduction step which was not needed for the continuum dataset. This disparity makes it strongly preferable to use the JCMT spectra for comparison to models, as line and continuum signals are obtained from the same JCMT data-product.

We also simulated the ALMA line-dilution problem using a signal of l:c = -2·10^{-4} in a circular 'cloud' of 8 arcsec diameter that was placed off-centre in the field, as if towards the planetary limb. Processing this simulation through CASA, we found the line signal was reduced by 37.5% for the whole cloud, if all telescope baselines were used. However, omitting baselines <33 m as in the real processing, 80-90% of the line signal was missing, for different parts of the cloud. Hence the ALMA line-to-continuum ratios suffer from significant line-loss in the case of few-arcsec scale smooth distributions, and under-estimate the true absorption depth. Given that we do not know the actual scales of cloud(s) of phosphine on the real planet, it is difficult to apply any corrections. In the main text, we discuss the maximum correction if the gas distribution is as smooth as the continuum – this structure is highly uniform, being only slightly fainter around the poles (Supplementary Figure 2).

As described in Methods, we verified (at modest significance) that the PH_3 absorption was reproduced in the wideband data, which arise from the same photons as the narrowband data. This analysis was made only to verify that the phosphine detection is not an artefact of our spectral-extraction processing. The original intent was to use the wideband data to measure line wings, but this could not be carried out due to the substantial spectral ripple.

Spectral contamination and uncertainties

Spectral line contaminants additional to SO_2

We checked whether absorption near 266.9445 GHz could be caused by another molecule within the Venus atmosphere. Supplementary Table 1 contains a list of all the molecular candidates within a ±80 MHz range of the PH_3 J 1-0 line – thus including transitions that might be detectable in our passbands even if they are not possible contaminants, and also allowing a check for species where transition frequencies have large uncertainties. The most likely contaminant for the PH_3 J 1-0 transition is the J=31 SO_2 line that we have ruled out as significant.

All other molecules that are known to be present in Venus are not spectrally active within the bandpass, and as such cannot be responsible for any absorption. The molecules in this category that we considered comprise: CO_2, N_2, H_2O, HDO, CO, H_2SO_4, $DHSO_4$, OCS, H_2S, O_3, HCl, DCl, SO, HF, DF, NO. Additional compounds of elements known to be present were also checked – phosgene; disulfur dioxide and isotopologues; other Cl, N, S, species including $ClSO_2$, ClOS, ClCN, HSD, HNSO, HOCl, DOCl, ClNO, NSCl, ClO_2, DNO, DCN. All of these had no transitions near our passband or only have data on their infrared transitions.

We also considered other molecules with transitions near the PH_3 1-0 line, but whose presence in the Venusian atmosphere would be equally extraordinary as phosphine. All known transitions that lie within 2 MHz of the PH_3 1-0 rest-frequency are listed in Supplementary Table 1 (upper section) – all the species apart from PH_3 and SO_2 are highly chemically implausible.

Some of these listed species may produce detectable astronomical signals in other contexts, e.g. envelopes of evolved stars and the interstellar medium. Two examples are an HC_3N line offset by +1.3 km/s with respect to PH_3 1-0, plus an SiS line that is further offset (at +3.1 km/s, just outside the tabulated range). The former line would be discrepant in velocity by ~4σ and the latter would be displaced into the wings of the phosphine line. HC_3N is a nitrile requiring high energy to make; it would form further bonds to the C-atoms at Venus' atmospheric density; it is probably unstable to UV photolysis; and it has the same problem as PH_3 in being a reduced (H-

bearing) gas species in an oxidised atmosphere. SiS gas would condense out at any temperature in Venus atmosphere, and also combine with trace water to form solids including SiO_2. Both are thus extremely improbable species – posing more problems to form that does PH_3. Further, these transitions are both from vibrationally-excited states, from energy levels at approximately 1500, 4300 K (HC_3N, SiS respectively) so the levels would be poorly populated in gas at < 300 K.

Strategies to confirm PH₃

Our recommendation is that phosphine transitions beyond the J=1-0 line be observed in the Venus atmosphere, so that its presence can be confirmed. This is unfortunately very difficult from ground-based facilities, as most transitions lie in challenging wavebands suffering from strong terrestrial atmospheric absorption. The J=3-2 transition of phosphine lies in ALMA Band 10, but it would require ~3 days of observation in first-octile conditions to achieve a 3σ statistical significance, for a ~1 km/s spectral bin at line minimum and assuming l:c ~2.5 10^{-4} (possibly an over-estimate, as the continuum will arise higher up at this frequency, potentially reducing the absorbing column above). This experiment would also be challenged by varying terrestrial conditions and observing parameters for Venus over the large number of days needed in practical operations. Other rotational transitions probably require a larger air- or space-borne telescope than are currently available.

Phosphine is also a strong absorber in the infrared, so ground-based telescopes capable of M- and N-band spectroscopy could in principle detect a portion of phosphine's strongest feature at 4-4.8 micrometres, and its broad band centered at 10 micrometres. We searched online archives of large infrared telescopes, specifically VIRTIS/VEX; IRTF (via the IRSA database) for the SpEX and ISHELL instruments plus TEXES (from private communications); and the ESO, Gemini and Subaru archives for all instruments, but did not find any relevant data for Venus. Further, the 4-4.8 micrometre region is likely to be completely dominated by CO_2 features. The most sensitive telescopes such as the James Webb Space Telescope (JWST) would have severe saturation and Sun-avoidance issues, so we recommend further investigation of ground-based instruments, possibly with adaptations to observing modes. We caution that mid-infrared and far-infrared observations might *not* detect any phosphine in absorption, depending on the height where the quasi-continuum signal is generated in these wavebands; e.g. at high altitudes, the molecules are expected to be photo-destroyed (Figure 5).

Adopted line frequency and sources of error in velocities in spectra

We adopt a line rest frequency for PH_3 1-0 of 266.9445 GHz. For the telescope configurations, we used an older frequency, 266.944662 GHz, but we corrected to the more recently-established rest-frame reference frequency in the data analysis. As a result, the central channel in each spectrum is not exactly at zero velocity of the center of Venus, but is offset by ~0.18 km/s. We neglect any resulting systematic in the calculation of centroid velocities of the lines (i.e. from the outcome that the velocity range has to be slightly asymmetric about zero, for integer channel numbers). Frequency scales of the correlators have a precision better than 0.1 km/s, and are treated as perfect in our analysis. There is no known value for a pressure-related (collisional) shift of the PH_3 1-0 rest frequency – values stated in catalogues are zero, but this is representing unknown rather than negligible. This shift will be orders of magnitude less than pressure broadening effects. Given the signal-to-noise in the spectra, we did not attempt to fit line profiles

with asymmetries representing collisional effects at moderate gas-pressure, such as Van Vleck-Weiskopf profiles. Such profiles were however included in the radiative transfer calculations.

ALMA observations were made in the reference-frame of Venus' center with respect to the observatory, but JCMT observations, while tracking the planet's position, adopted zero velocity as being in the rest frame of the telescope. Venus' velocity relative to JCMT was tabulated (from the JPL Horizons tool) for the mid-point of each ~30 minute observation, and each observation was shifted to the Venus frame in analysis (see values in Supplementary Software 1). The line was located at +13.49 to +14.06 km/s in the JCMT telescope-referenced spectra (mean of +13.8 km/s), sufficient to shift the absorption feature away from any terrestrial line at v = 0 km/s, in the highly unlikely event of a small terrestrial plume of phosphine entering the on-source telescope beam. The uncorrected velocity-shifts during each of the JCMT observations are negligible (<0.05 km/s). For the ALMA observations, the relative velocity of Venus was in the range +11.6 to +12.0 km/s, so again no terrestrial contamination is plausible. (There are also no catalogued transitions at a suitable frequency that could mimic phosphine on Venus after applying the velocity-shift between the two planets.) The rotation of Venus' upper atmosphere at ~0.1 km/s cannot be detected within the signal-to-noise of our spatially-resolved ALMA data.

Photochemical model

As noted in the Methods, previously published models of the Venusian atmosphere did not include the scavenging effect of PH_3, and so we found it necessary to develop our own model. Additional publications are planned on this work, expanding on the description below.

We employ the 1D photochemistry-diffusion code ARGO[46] to solve the atmospheric transport equation for the steady-state vertical composition profile. The model took the handful of known reactions between PH_3 and the major reactive Venusian species O, Cl, OH, and H, and combined them with the previously published Venus atmospheric networks of Krasnopolsky[49,57] and Zhang[50], and the network of Rimmer & Rugheimer[48]. This whole-atmosphere model allows us to self-consistently assess the lifetime of PH_3 throughout the atmosphere. The model accounts for photochemistry, thermochemistry and chemical diffusion.

We employ a 1D photochemistry-diffusion code, called ARGO[46], to solve for atmospheric transport. ARGO is a Lagrangian photochemistry/diffusion code that follows a single parcel as it moves from the bottom to the top of the atmosphere, determined by a prescribed temperature profile. The temperature, pressure, and actinic ultraviolet flux are updated at each height in the atmosphere. In this reference frame, bulk diffusion terms are accounted for by time-dependence of the chemical production, P_i (cm^3 s^{-1}), and loss, L_i (s^{-1}), and so below the homopause, the chemical equation being solved is effectively:

$$\frac{\partial n_i}{\partial t} = P_i[t(z, v_v)] - L_i[t(z, v_z)]n_i, \qquad\qquad M1$$

where n_i (cm^{-3}) is the number density of species i, t (s) is time, z [cm] is atmospheric height, and $v_z = K_{zz}/H_0$ (cm/s) is the effective vertical velocity due to Eddy diffusion, from the Eddy diffusion coefficient K_{zz} (cm^2 s^{-1}). The model is run until every major and significant minor species (any with $n_i > 10^5$ cm^{-3}) agrees between two global iterations to within 1%. We have modified the UV transport calculation in two ways. First, we ignore the absorption of SO_2 for the

first three global iterations, and include it afterwards. This seems to help the model to converge. In addition, we have included a 'mysterious absorber' with properties[47]:

$$\frac{d\tau}{dz} = 0.056/km \; e^{-(z-67 \, km)/3 \, km} e^{-(\lambda - 3600 \, \text{Å})/1000 \, \text{Å}}, \qquad z > 67 \; km;$$

$$\frac{d\tau}{dz} = 0.056/km \; e^{-(\lambda - 3600 \, \text{Å})/1000 \, \text{Å}}, \qquad\qquad 58 \; km \leq z \leq 67 \; km;$$

$$\frac{d\tau}{dz} = 0, \qquad\qquad\qquad\qquad\qquad z \leq 58 \; km;$$

With these conditions, using the photochemical network described below, it took 33 global iterations for the calculations to converge.

Photochemical network for Venus

For our chemical network, we use STAND2019[48], which includes H/C/N/O species. We have also added a limited S/Cl/P network relevant for the Venusian atmosphere by copying the low atmospheric network of Krasnopolsky[47,49] and the middle atmosphere network of Zhang[50], and supplementing those networks with the following reactions (see ref. 10 for literature sources):

$PH_3 + M \rightarrow PH_2 + H + M,$ $\qquad k_0 = 3.4 \times 10^{-8} \; cm^3 \; s^{-1} \; e^{-35644 \, K/T};$

$\qquad\qquad\qquad\qquad\qquad\qquad k_\infty = 1.91 \times 10^{18} \; s^{-1} \; e^{-40063 \, K/T};$

$PH_3 + H \rightarrow PH_2 + H_2,$ $\qquad k = 7.22 \times 10^{-11} \; cm^3 s^{-1} e^{-884 \, K/T};$

$PH_3 + O \rightarrow Products,$ $\qquad k = 4.75 \times 10^{-11} \; cm^3 \; s^{-1};$

$PH_3 + OH \rightarrow PH_2 + H_2O,$ $\qquad k = 1.61 \times 10^{-11} \; cm^3 \; s^{-1};$

$PH_3 + Cl \rightarrow PH_2 + HCl,$ $\qquad k = 2.4 \times 10^{-10} \; cm^3 \; s^{-1};$

$PH_3 + h\nu \rightarrow PH_2 + H$
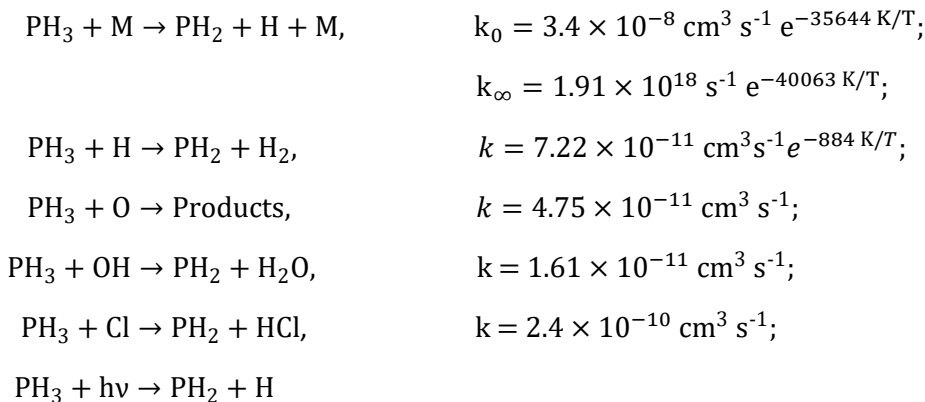
We calculate the rate constant for $PH_3 + M \rightarrow PH_2 + H + M$, where M is any molecule, as described below. For the reaction, $PH_3 + O \rightarrow Products$ has products with branching ratios (when T < 500 K) of >90% PH_2O + H and <10% PH_2 + OH. Because virtually no PH_2 is restored to PH_3 in the photochemical model, we do not explicitly include PH_2O in the chemical network, but simply treat the reaction of PH_3 + O as a loss of PH_3 with the above given rate constant.

For the reactions we include not involving PH_3, we use the networks of Krasnopolsky[47] and Zhang[50] with the following modifications. The network of Krasnopolsky include prescribed reverse reactions. We neglected these, including the forward reactions and the thermochemical constants from Burcat[51] for calculating the reverse reactions for those species already included in STAND2019, as well as reactions that include the species S, S_2, S_3, S_4, S_5, S_6, S_7, S_8, HS, SO, ClO, ClS, Cl_2, H_2S, OCS, SO_2, SO_3, S_2O, HOCl, ClCO, Cl_2S, Cl_2S_2, HSO_3, H_2SO_4, PH_2 and PH_3, in the manner described by refs. 46,52. We added reverse reactions for the reactions from the Zhang[50] middle atmosphere network wherever possible. In addition to these reactions, we include condensation of S_n species[53] and sulfuric acid H_2SO_4[54].

We add removal of SO_2 into the clouds in order to match the top boundary conditions from the lower atmosphere models[47] to the bottom boundary conditions for the middle atmosphere models, where the SO_2 is depleted by orders of magnitude[50]. Bierson and Zhang accomplished this by depleting SO_2 via oxidation to SO_3 and removal by reaction with H_2O to form sulfuric acid[55]. The SO_2 could only be brought into agreement with observation by decreasing K_{zz} within the cloud layer and fixing H_2O to be equal to observed concentrations throughout the atmosphere. We do not fix the H_2O concentrations, and so instead have depleted SO_2 by including rainout with a Henry's Law approximation modified as described by Sander (ref. 56, their Section 2.7), with the pKa of the resulting sulfurous acid being 1.81 and the pH of Venus's clouds as -1.5. It should be noted that the Henry's Law constants from Sander[56] are for liquid water, and not for sulfuric acid droplets. Nevertheless, incorporating this loss term brings the SO_2 curve into better agreement with observation, and may instead be interpreted as approximating photochemical loss of SO_2 via a different mechanism or series of reactions.

Thermal Decomposition of Phosphine

Consideration of the thermal decomposition of phosphine is important because concentrations of radicals below the clouds of Venus are trace, $<<$ 1 ppb. Estimated concentrations of radicals below the clouds are very uncertain, and even with the largest published predictions[47] for radical concentrations in the lower atmosphere of ~ 1000 cm^{-3}, thermal decomposition dominates PH_3 destruction and therefore is determinative of the lifetime near the surface of Venus. The thermal decomposition of PH_3 has been considered theoretically[65]. Theoretical values of k_{uni} (s^{-1}) and k_∞ (s^{-1}) are given as[65]:

$$k_{uni} = 3.55 \times 10^{14} \text{ s}^{-1} e^{-35644 \text{ K}/T}$$

$$k_\infty = 1.91 \times 10^{18} \text{ s}^{-1} e^{-40063 \text{ K}/T}$$

but no value for the rate constant at the low-pressure limit, k_0 (cm^3 s^{-1}), is given. This rate constant needs to be determined in order to calculate the rate constant over a wide range of pressures using the Lindemann expression:

$$k = \frac{k_\infty}{1 + k_\infty/(k_0[M])} \qquad R3$$

where [M] is the number density of the third body, in our case $[M] = n$, where n (cm^{-3}) is the atmospheric number density. The rate constant at the low pressure limit can be estimated by considering that k_{uni} was calculated for 1300 bar and 900 K, so $[M] = 1.07 \times 10^{22} cm^{-3}$, and solving Equation ($R3$) with $k = k_{uni}$. Doing so yields:

$$k_0 = 3.4 \times 10^{-8} \text{ cm}^3 \text{ s}^{-1} e^{-35644 \text{ K}/T} \qquad R4$$

An alternative way to estimate k_0 from k_∞ is to perform a simple conversion of units, with $k_0 = kT/(1 \, bar) \, k_\infty$, which gives:

$$k_0 = 2.6 \times 10^{-4} \text{ cm}^3 \text{ s}^{-1} \left(\frac{T}{300 \, K}\right) e^{-40063 \text{ K}/T} \qquad R5$$

Finally, we can consider the decomposition of NH_3 as an analogue of the decomposition of PH_3. In this case, the low-pressure limit for NH_3 has been experimentally determined over a temperature range of 1740-3300 K[66]. We assume that the prefactor is the same for PH_3 and that the only difference is the activation energy, for which we compare the activation energy at the

high pressure limit of 40063 K for PH_3[65] to the activation energy at the high-pressure limit of 48840 K for NH_3[65], and multiply the ratio of these activation energies to the measured activation energy for NH_3 at the low-pressure limit of 39960 K[66] to find:

$$k_0 = 7.2 \times 10^{-9} \text{ cm}^3 \text{ s}^{-1} e^{-32778 \text{ K}/T} \qquad \qquad R6$$

The timescales for thermal decomposition derived from these rate constants, along with the timescale using only k_∞, are plotted in Supplementary Figure 8. Since our first estimate, Equation (*R4*), yields the longest timescale, and will therefore be most favorable for abiotic PH_3 scenarios, we use that value.

In total, the network includes 460 species and 3406 forward reactions, including 173 photochemical reactions. For a full description of the photochemical network models that we used in this paper, see ref. 35.

Initial and boundary conditions

In modelling the Venusian atmosphere, we follow refs. 47,57 in taking the temperature-pressure (TP) profile from the Venus International Reference Atmosphere (VIRA). Specifically, we use previously published TP profiles of ref. 58 for the deep atmosphere profile (0-32 km) and for the altitudes between 32-100 km, where we use the 45 degrees latitude profile. For the altitudes between 100-112 km we use the VIRA dayside profile from ref. 59. Supplementary Figure 8 shows the temperature-pressure profile adopted in this work. We similarly follow refs. 47,57 in the Eddy diffusion profile, taking it to be constant at $2.2 \cdot 10^3$ cm^2 s^{-1} for z <30 km, $1 \cdot 10^4$ cm^2 s^{-1} for z = 47-60 km, $1 \cdot 10^7$ cm^2 s^{-1} for z >100 km, and connected exponentially at intermediate altitudes. Supplementary Figure 8 shows the Eddy diffusion profile adopted in this work (see also below, under Photochemistry in the atmosphere).

We take fixed surface boundary conditions from ref. 47 for the major atmospheric species, and with initial surface boundary conditions from ref. 47 for minor species, radicals and atoms, except for PH_3. Initial surface abundances for our model are shown in Supplementary Table 2.

We include a source of PH_3 in the clouds, with flux:

$$\Phi(z) = 0.5\Phi_0 \left[\tanh\left(\frac{z - 45 \text{ km}}{2 \text{ km}}\right) \tanh\left(\frac{65 \text{ km} - z}{2 \text{ km}}\right) + 1\right]$$

where $\Phi(z)$ (cm^{-2} s^{-1}) is the PH_3 flux at height z (km), and $\Phi_0=10^7$ (cm^{-2} s^{-1}) is assigned to reproduce the 10 ppb PH_3 concentrations.

Validation and limits of the model: Comparison of the Venus chemical kinetics model with atmospheric observations

The model predictions for a variety of species, CO, O_2, OCS, H_2O, SO_2, H_2S, HCl, S_3, SO, and PH_3, compared to observations (Supplementary Table 3) are plotted in Supplementary Figure 9. The profiles for all species agree with observations within an order of magnitude in concentration, within 5 km height, except for the ALMA SO_2 data (ref. 27; this work), water vapor and O_2. Photolysis of water is very efficient for our model, and depletion by reaction with SO_3 is significant, and our model's predicted water vapor drops off rapidly above 70 km, leading to a discrepency between observed H_2O and model H_2O of several orders of magnitude. This discrepancy is accompanied by higher concentrations of OH and O above 70 km, and so we

probably underestimate the lifetime for phosphine above 70 km. However, the lifetime of phosphine at these heights is very short, on the order of days to seconds, for all published models of Venus's middle atmosphere (e.g. by Zhang[50] and Bierson & Zhang[55]). Our model also predicts too much O_2 in the middle atmosphere of Venus, with similar concentrations as Zhang[50] and Bierson & Zhang[55].

We consider the possibility that our model contains an idiosyncrasy or error that leads to significant underestimates of PH_3 lifetime, and hence overestimates the difficulty of abiotic buildup. To assess this possibility, we repeat our calculations of PH_3 lifetime and required production rates using concentration profiles of H, OH, O, Cl, and SO_2 drawn from Bierson & Zhang[55] (aided by C. Bierson, personal communication, 08/02/2019). This model excludes PH_3; consequently, it may overestimate lower-atmosphere radical abundances and underestimate PH_3 lifetimes. Use of these radical profiles, instead of the profiles drawn from our model, result in PH_3 lifetimes becoming short ($<10^3$ s) at an altitude of 71 or 80 km instead of 63 km in our model, depending on which of the scenarios from Bierson & Zhang we adopt (their nominal vs. their low $K_{zz}+S_8$ scenarios). However, this change in destruction altitude does not affect the upper limits on lifetime we calculate strongly enough to affect the conclusions of this paper.

For further description of the models used in this paper also see ref. 35.

Potential pathways for phosphine production.

We discuss the potential pathways for phosphine production in the Venusian environment and why PH_3 production is ruled out for conditions of the Venusian atmosphere, surface, and subsurface. The discussion is summarized in Table S4. For more details, see ref. 35.

Phosphine lifetime

We estimate the rate of destruction of phosphine as discussed above.

The photochemical lifetime of PH_3 can be high in the deep atmosphere, but is always low in the high atmosphere where UV photolysis and its concomitant radicals efficiently destroy PH_3. In the deep atmosphere, transport to the upper atmosphere will limit PH_3 lifetime. To account for the effects of transport on PH_3 lifetime, we calculate the transport timescale for PH_3 at altitude z_1 due to eddy diffusion, via $t_{transport}=\Delta z^2/K_{zz}$, where K_{zz} is the eddy diffusion coefficient, and $\Delta z=z_0-z_1$, where z_0 is the vertical altitude at which PH_3 lifetimes are short due to photochemistry. In our photochemical model above, $z_0 = 63$ km; however, in other models, z_0 can be as high as 80 km (C. Bierson, personal communication, 07/24/2019). The pseudo-first order rate constant of PH_3 loss due to eddy diffusion is thus $1/ t_{transport}= K_{zz} /\Delta z^2$. We conservatively adopt $K_{zz}=K_{zz}(z_1)$; since Kzz is monotonically nondecreasing with z, this underestimates K_{zz}, overestimates $t_{transport}$, and underestimates the destruction rate. We adopt the lower of the transport timescale to 63 km and the photochemical lifetime as our overall lifetime.

Photochemical production of phosphine

The maximum possible potential rate at which phosphine could be produced photochemically is estimated as follows. We created a network of reactions for which kinetic parameters are known[67] that could lead from H_3PO_4 (phosphoric acid) to PH_3 (phosphine), by reaction with radical species in the Venusian atmosphere (Supplementary Figure 7). We know from the thermodynamic data summarized below (and presented in detail in ref. 35) that reaction with

stable species such as H_2 cannot yield phosphine in adequate amounts from thermodynamic arguments. Where reactions were possible but no kinetic data for the phosphorus species was known, homologous nitrogen species reaction kinetics were used instead. This was validated by comparing reaction of analogous nitrogen and phosphorus species: the N=O and P=O bond energies are similar, transition state energies for cleavage of H-N=O and H-N=P are similar, HOMO/LUMO structures (which relate to reaction pathways) are similar, and HNO_3 and HNO_2 have similar radical reaction kinetics to HPO_3 and HPO_2 species respectively. By contrast, hydrogen abstraction from NH_3 is very much slower than hydrogen abstraction from PH_3, reflecting different bond strengths; however kinetic data for P species is known for hydrogen abstraction reactions. Kinetic data were obtained from the NIST kinetics database[60], supplemented by refs. 67 and 68.

The kinetics of each reaction was calculated for densities of radical species calculated in the photochemical code above. The *maximum possible* rate of phosphine production was then calculated with the following assumptions:

- that there were no 'back' reactions (i.e. all reactions that could happen were ones that reduced phosphorus atoms)

- for *each* reaction, the concentration of phosphorus species taking part was the concentration of *all* phosphorus species in the atmosphere.

The maximum rate through the network is therefore the maximum rate through any path through the network, and the rate through any path is the minimum of each individual reaction rate along that path. This maximum possible rate was compared with the rate needed to balance photochemical destruction of phosphine. The steady-state abundance in this case is:

$$f(PH_3) = \frac{P_{abiotic}(PH_3)}{L(PH_3)n}$$

where $P_{abiotic}(PH_3)$ (cm^{-3} s^{-1}) is the maximum abiotic production rate of PH_3, n (cm^{-3}) is the total gas number density, and

$$L(PH_3) = \max\{L_R, 1/\tau_{transport}\}$$

is the PH_3 destruction rate constant (s^{-1}). Here, L_R is the destruction rate of PH_3 according to our photochemical model, and $1/\tau_{transport} = K_{zz}/\Delta z^2$, as defined above.

Equilibrium thermodynamics in the atmosphere and surface

Chemical thermodynamics is a robust way to determine if a reaction favors the net production of the product at equilibrium (i.e. does not require an input of energy from the environment to drive the net conversion of reagents to product). A thermodynamically possible reaction may be prohibited by kinetic barriers, but a thermodynamically impossible reaction will not be a spontaneous net producer of a reaction product no matter what the reaction kinetics. In other words, while thermodynamics always correctly predicts whether a given process is favored (is spontaneous from the thermodynamic point of view), it does not tell if the chemical process will take place at an observable rate. (Apropos the kinetic model, we note that the reaction of hydrogen *atoms* with H_3PO_4 to form PH_3 is thermodynamically favoured.)

Considering the atmosphere and surface of Venus, we created a list of chemicals, their concentrations, and reactions, for all potential PH_3 production pathways. To produce phosphine

from the oxidized phosphorus species expected on Venus, a phosphorus-containing compound must be reduced. We therefore considered examples of all types of phosphorous-containing compounds as sources of phosphorus, and as reducing agents all atmospheric components which could in principle behave as reducing agents for which an atmospheric concentration has been measured or modeled, and a sample of Fe(II) solid compounds which could act as surface reducing agents. We used literature values for standard free energy and the concentrations of reactants. Temperatures and pressures come from the Venusian Standard Atmosphere. Activities were calculated using Berthelot's equation[69] and literature values for critical temperature and pressure for gases. We have calculated Gibbs Free Energy[70,71] of reaction to estimate the possibility of phosphine formation (Supplementary Figure 7), recalling that negative values mean the reaction happens spontaneously. Reactions of P_4O_6, P_4O_{10}, H_3PO_4 and H_3PO_3 were considered (the last of these only in solution phase in the clouds), as well as surface reduction of phosphate minerals. Our calculation considered 8 phosphorus-reducing species, in ~75 reactions. Reactions with gases were calculated with a high or a low gas concentration, derived from published models[47,57,72-76], in all combinations., in different temperature/pressure regimes, leading to ~3840 conditions tested for each reaction. Thermodynamics was only followed to the cloud tops, after which freeze-out of phosphorus species makes reactions of stable phosphorus compounds implausible.

Not surprisingly, for an oxidized atmosphere with little P, none of the reactions favor the formation of phosphine, on average having a free energy of reaction of +100kJ/mol (Supplementary Figure 7). For further details on thermodynamic modeling of phosphine production in the Venusian atmosphere see ref. 35 .

As an example of our approach, we present a calculation for phosphorous acid (H_3PO_3). This compound will spontaneously decompose on heating to form phosphoric acid and phosphine; this is a standard laboratory method for making phosphine . Phosphorous acid is not stable in gas phase, but could in principle be formed in cloud droplets by reduction of phosphoric acid. We calculated the equilibrium fraction of phosphorus present as H_3PO_3 in droplets in Venus' cloud assuming conditions as described above. H_3PO_3 is a tiny fraction of the total phosphorus inventory; if phosphorus was present as 1 molar H_3PO_4 in droplets, then the concentration of H_3PO_3 would be ~6.10^{-17} molar at 47 km (the base of the clouds, which is below our minimum detection altitude), and at >53 km (the approximate minimum altitude of the candidate detection of PH_3) would be ~10^{-20} molar. If we assume a total volume of cloud material of $1.04 \cdot 10^{10}$ m^3 (calculated from the droplet sizes, droplet abundances and cloud depth), the clouds above 47 km would contain ~44 milligrams of H_3PO_3 in the entire Venusian atmosphere. Reduction of phosphate to phosphite and subsequent disproportionation of phosphite is therefore not a plausible source of phosphine.

We investigated possible chemical reactions involving subsurface phosphate-containing minerals that may produce phosphine by reduction. The chemical composition of the subsurface and the deep interior of Venus is poorly known. It is assumed to be similar to the chemical composition of the Earth's crust and mantle, mainly due to the similarity of Earth and Venus in terms of the size and the overall bulk density of two planets[77]. The Venusian crust is largely basalt, which suggests that Venusian mantle is likely similar in chemical composition to Earth's mantle[75,77,78].

Detailed modelling of the subsurface chemistry is not practical. A convenient simplification of this complexity with respect to the redox state of the crust, and hence the potential for the crust to support redox reactions, is the concept of oxygen fugacity (fO_2)[61]. In brief, f(O_2) is the

notional concentration of free oxygen in the crustal rocks. A higher oxygen fugacity of the rock means a more oxidized rock and a lower probability of reduction of phosphates.

We use the concept of oxygen fugacity[61] to estimate the likelihood of phosphine production from phosphate subsurface minerals. We model the equilibrium between phosphate and phosphine under oxygen fugacity buffers QIF, WM, IM, FMQ or MH (terrestrial crustal rocks typically have $f(O_2)$ between FMQ and MH). Calculations were performed for temperatures between 700K and 1800K, at 100 or 1000 bar and with 0.01%, 0.2% and 5% water. We conclude that oxygen fugacity of plausible crust and mantle rocks is 8-15 orders of magnitude too high to support reduction of phosphate. Degassing of mantle rocks would therefore produce only trivial amounts of phosphine compared to their total phosphorus content.

Our fugacity calculations are supported by observations that phosphine is not known to be produced by volcanoes on Earth. Calculations on the production of PH_3 through volcanism on a simulated anoxic early Earth showed that only trace amounts of volcanic PH_3 can be created through this avenue; the predicted maximum production rate is only 102 tons per year[79]. We note that the estimation of the maximum production of PH_3 through the volcanic processes reported by ref. 79 is made under the assumption of a highly reduced planet, which provides favorable conditions for PH_3 volcanic production. The volcanic production of PH_3 in more oxidized planetary scenarios is even more unlikely.

Lightning

Lightning may be capable of producing a plethora of molecules that at first glance are energetically unfavorable to make.

We assume for simplicity that the energy delivered by a lightning bolt leads to a complete atomization of chemicals within a droplet or within the gas inside the volume of the lightning stroke. We further assume that subsequent recombination of atoms into stable chemicals proceeds at random, and is dependent solely on the composition of Venus' clouds and atmosphere and the number density of the atoms in the resulting plasma.

Under such assumptions, the maximum amount of phosphine produced in 1 year is $3.38 \cdot 10^8$ grams. If this accumulated in Venus' atmosphere for a full Venusian year without any destruction, it would reach a partial pressure of 0.00076 parts per trillion, much lower than ~10 ppb phosphine concentration that we model in the Venusian atmosphere.

The above calculations are in agreement with several studies on the formation of reduced phosphorus species, including PH_3, as a result of simulated lightning discharges in laboratory conditions. The laboratory experiments suggest that in principle reduction of phosphate to phosphine through lightning strikes is extremely inefficient[80,81], further strengthening the argument that lightning discharges cannot be responsible for the observed phosphine concentrations in the Venusian atmosphere.

Meteoritic delivery

Iron-nickel meteorites are known to contain reduced species of phosphorus. We calculate possible delivery fluxes on Venus to exclude phosphine production by meteoritic delivery.

The current accretion rate of meteoritic material to the Earth is of the order of 20-70 kilotonnes/year[82]. Approximately 6% of this material is in the form of phosphide-containing

iron/nickel meteorites[83] which contain an average of 0.25% phosphorus by weight[84]. If we assume that hydrolysis of $(Fe,Ni)_3P$ phosphides to phosphine is 100% efficient, that would deliver a maximum of ~10 tonnes of phosphine to the Earth every year, or about 110 milligrams/second. Assuming Venus accretes phosphides at a similar rate, and assuming a photochemical destruction rate of phosphine is as shown in Figure 5, and that all the phosphine is deposited at 50-60 km (where destruction is slowest), the concentrations of PH_3 is:

$$f(PH_3) = \frac{N_A S_M \tau(PH_3)}{\mu(PH_3) \, n\Delta h \, 4\pi R_{Venus}^2} \qquad R1$$

where $\mu(PH_3) = 34$ g/mol is the molar mass of PH_3, $n = 6.5 \times 10^{18}$ cm^{-3} is the gas density at 60 km, $\Delta h = 10$ km, $R_{Venus} = 6052$ km is the radius of Venus, $N_A = 6.022 \times 10^{23}$ is Avagadro's constant, $\tau(PH_3) = 10^{10}$ s and $S_M = 0.11$ g/s is the amount of PH_3 delivered per second to Venus according to the above approximation. Applying all these values, we find:

$$f(PH_3) = 6.5 \times 10^{-13} \qquad R2$$

This is orders of magnitude lower than the observationally-constrained ~20 ppb phosphine concentrations, regardless of the photochemical model in question. We note that the above calculations are also in agreement with previous estimations of the phosphine production through meteoritic delivery, which were also found to be negligible[84].

Other endergonic processes are covered in ref. 35.

Horizontal Transport, Chemical Timescales and Latitudinal Variation of Phosphine

As discussed above, the lifetime of PH_3 in the atmosphere of Venus is constrained by photodissociation in the upper atmosphere, thermal decomposition near the surface, and diffusion in between. The constraints these three processes provide are similar across all the photochemical models. Further constraints involving radical chemistry are highly model dependent. We can use the latitudinal variation of PH_3 to constrain the lifetimes of PH_3 within the atmospheric regions where radical chemistry dominates. We do this by comparing the model-dependent chemical lifetimes of PH_3 to zonal and meridional velocities. If the velocities are too great, compared to chemical lifetimes, mixing will be efficient, and regardless of the source of PH_3, it will be well-mixed. The minimum scale over which variation is expected is then:

$$L = v\tau_{chem} \qquad R7$$

where v (m/s) is the either the meridional or zonal velocity in question and τ_{chem} (s) is the chemical lifetime of PH_3. We consider that observable latitudinal variation implies that $L \lesssim R_{Venus}$, and plot the velocity above which PH_3 would be well-mixed, in Supplementary Figure 9. Given the constraints on zonal and meridional velocity given by cloud tracers[63,64], the latitudinal variation is somewhat unexpected. It implies either that (a) the PH_3 being observed is largely at altitudes above 60 km *and* that this work and Krasnopolsky[47,49] better represent Venusian radical chemistry, or (b) that there is some yet unknown mechanism that more rapidly destroys PH_3 within the cloud layer. Further observations will help constrain both the robustness of the latitudinal variation and its vertical profile. In addition, further laboratory experiments exploring PH_3 stability will help to identify what other mechanisms may be responsible for its destruction within the cloud layer.

PH₃ and hypotheses on Venusian life

The Venusian surface is widely believed to be uninhabitable. However, the clouds of Venus offer temperate conditions, and the possibility of life in the Venusian clouds has been discussed for decades[16,85-87]. It has been speculated that the unknown and variable ultraviolet opacity (currently being monitored by the *Akatsuki* spacecraft) is due to life particle pigments[17] though chemical processes may be the source[88].

To this discussion, we add that trace PH_3 in Earth's atmosphere is uniquely associated with biological and anthropogenic activity[10,18,89], and we have proposed that any detectable phosphine found in the atmosphere of a rocky planet is a promising sign of life[10]. Terrestrial life produces this highly reducing, endothermic gas even in an overall oxidizing surface environment, and notably the biological production of phosphine is found to be favored by cool, acid conditions[18]. Thus, phosphine is a biosignature of some interest for the cool but hyper-acidic conditions of Venusian clouds.

Computer models of Venus[90,91] have shown that a habitable surface with liquid water could have persisted up to 715 million years ago (Mya), and *Magellan* data indicate complete resurfacing after this (~500 ±200 Mya[92], perhaps taking ~100 Myr[93]). Such effects would radically alter the planetary environment, and it has been widely suggested that, as the surface was rendered inhospitable, life could have gradually colonized the clouds, eventually becoming an entirely aerial biosphere. As a parallel for such suggestions, Earth has a metabolically-active aerial biosphere[94,95].

Initial modelling based on terrestrial biochemistry suggests that biochemical reduction of phosphate to phosphine is thermodynamically feasible under Venus cloud conditions[35]. Biological phosphine production on Venus is likely to be energy requiring[18]. However, life can make substantial energy investment into compounds that provide important biological functionality. There are many potential useful biological functions including signaling, defense, or metal capture for which phosphine has useful properties[89], so endergonic biosynthesis cannot be ruled out.

Supplementary Table 1. Upper section: list of molecular transitions near the PH$_3$ 1-0 line (highlighted in green), from the Cologne Database for Molecular Spectroscopy (CDMS). The columns list the rest frequencies and their uncertainties, the energy of the lower level of the transition, the transition's quantum numbers, and the chemical species. This selection shows all transitions within 2.5 MHz of the PH$_3$ 1-0 frequency – any transition outside this range would yield a Doppler shift differing from the PH$_3$ 1-0 line by >5σ (for σ ~0.5 km/s: quadratic combination of uncertainties for the ALMA whole-planet spectrum, Table 1). Telluric absorption (at frequencies offset by the Venus-Earth Doppler-shifts) can be ruled out because telluric line widths exceed ~100 km/s (as verified through a feature seen by ALMA, see section above on ALMA data acquisition). The only listed molecule that is plausible for Venus is SO$_2$ (transition highlighted in yellow) and the potential contamination-levels are illustrated in Figure 4. Lower section: list of molecules that we considered as possible contaminants for the PH$_3$ 1-0 line (highlighted in green). Abundances are listed for Venusian molecules that have been measured in-situ or modelled[23]. UNK denotes molecules not been previously measured or predicted on Venus; the estimates in brackets are based on Earth's isotopic ratio. The list covers molecules spectrally active within 80 MHz of the PH$_3$ 1-0 frequency, with listed quantities including transition wavenumber (in GHz, in vacuum), strength (in cm^{-1} / (molecule·cm^{-2}), at T=296 K), and rotational quantum numbers (J). The entry in yellow highlights the most likely contaminant, SO$_2$. All other molecules considered are not expected to be present in Venus at sufficiently high concentrations for their listed weak transitions to be likely absorption candidates ('unlikely contributors'). Other species present or possible but with no spectral activity in the passband are collated in the final two rows. Spectral data are from the GEISA[23], HITRAN[24] and ExoMol[25] databases, and from ref. 26.

freq. (MHz)	error (MHz)	E$_{lower}$ (K)	upper level	lower level	species
266942.087	0.03	26.3	7 2 5	7 1 7	CHD2CN
266942.422	0.199	418.6	39 23 16	38 23 15	Glycine, conf. I
266942.422	0.199	418.6	39 23 17	38 23 16	Glycine, conf. I
266942.483	2.449	206.2	33 12 22	33 8 25	i-C3H7CN-13C1
266942.540	16.21	912.3	65 20 45	64 21 44	s-trans-Propenoic acid
266942.666	0.012	709.4	39 27 13 0 0	39 25 15 0 0	CH3COOH, vt=0
266942.719	0.120	61.9	8 5 3	7 6 2	c-CC-13-H4O
266943.075	0.007	1132.7	82 64 18	81 65 17	2-CAB, v=0
266943.075	0.007	1132.7	82 64 19	81 65 16	2-CAB, v=0
266943.325	0.0012	613.1	30 9 21	31 8 24	SO2,v=0
266943.407	0.009	1450.4	29 0 0	28 0 0	HC3N, v7=4/v5=v7=1
266943.525	0.012	513.0	29 920 2 0	2920 9 1 0	CH3COOH, Dvt<>0
266943.536	0.086	1095.4	56 16 40 2	55 17 39 1	CH3OC-13-HO, vt=0,1
266943.547	0.067	1133.3	48 22 27 2 0	47 30 17 1 0	CH3COOH, Dvt<>0
266944.038	0.013	998.3	58 16 43 1	57 17 40 1	s-Propanal, v=0
266944.457	0.004	376.9	46 12 35 0	46 10 37 1	a'GG'g-1,3-Propanediol
266944.510	0.443	1785.6	A0 25 76 0	A0 23 77 1	gGG'g-1,3-Propanediol
266944.514	0.0002	0.0	1 0	0 0	PH3
266945.085	0.153	604.1	80 18 62	81 17 65	AA-n-C4H9CN
266945.085	0.153	604.1	80 18 63	81 17 64	AA-n-C4H9CN
266945.102	0.003	192.8	30 3 27	29 3 26	CH2D(oop)CH2CN
266945.315	0.005	888.5	52 17 35	53 16 38	CH3C-13-H2CN, v=0
266945.315	0.005	888.5	52 17 36	53 16 37	CH3C-13-H2CN, v=0
266945.781	0.057	809.4	70 33 37	70 32 38	OC(CN)2
266945.781	0.057	809.4	70 33 38	70 32 39	OC(CN)2
266946.021	0.012	998.3	58 16 43 0	57 17 40 0	s-Propanal, v=0
266946.398	0.02	809.4	38 17 22 2 2	37 18 19 2 1	CH3COOH, vt=2
266946.678	4.977	1519.2	88 9 79	88 8 80	g-n-C3H7CN, v28=1
266946.960	0.0023	123.9	28 5 23	28 2 26	cis-S2O2

species	type	abundances on Venus (estimates and/or altitude-dependent)	freq. (MHz)	strength (cm^{-1} / mole.cm^{-2}))	quanta (J$_{upper}$ - J$_{lower}$)	additional lines	Notes
PH$_3$	molecule	UNK	266944.5	1.27E-22	1-0		target line
^{32}S^{16}O$_2$	molecule	~50 ppb – ~150 ppm (Supplementary Table 3)	266943.3 267006.8	3.18E-23 4.56E-24	30-31 15-16		modelled contaminant
^{16}O^{16}O^{17}O	isotope	UNK (ppb/ppt)	266925.2	5.21E-27	23-23	+15 weaker lines in range	unlikely contributor
^{16}O^{17}O^{16}O	isotope	UNK (ppt)	266932.7	5.21E-27	23-23	+12 weaker lines in range	unlikely contributor
^{32}S^{16}O$_3$	molecule	UNK (ppb)	267024.6 266970.6	4.91E-28 5.82E-28	60-59 47-48		unlikely contributor
^{14}N^{16}O$_2$	molecule	UNK	266926.4	5.08E-27	32.5-33.5		unlikely contributor
NH$_3$	molecule	UNK	266992.0	1.40E-26	3-3		unlikely contributor
H^{14}N^{16}O$_3$	molecule	UNK	266974.5	8.95E-25	29-29	+95 weaker lines in range	unlikely contributor
H^{15}N^{16}O$_3$	isotope	UNK	266952.9	4.62E-27	14-15	+2 weaker lines in range	unlikely contributor
^{12}CH$_3$^{16}OH	molecule	UNK	266871.9	6.83E-24	14-15	+2 weaker lines in range	unlikely contributor
^{15}N^{14}N^{16}O	isotope	UNK	~266995 (only 4 sig. fig. listed)	2.46E-25	11-10		unlikely contributor
CO$_2$, N$_2$, H$_2$O, HDO, CO, H$_2$SO$_4$, DHSO$_4$, OCS, H$_2$S, O$_3$, HCl, DCl, SO, HF, DF, NO							known on Venus, but no spectral activity in passband
ClCO$_2$, S$_2$O (+ isotopologues), ClSO$_2$, ClOS, ClCN, HSD, HNSO, HOCl, DOCl, ClNO, NSCl, ClO$_2$, DNO, DCN							compounds of elements present on Venus; no spectral activity near passband or no data on millimetre transitions

Supplementary Table 2. Initial surface conditions adopted for the atmospheric chemistry.

Species	Mixing Ratio
CO_2	0.96
N_2	0.03
SO_2	1.5×10^{-4}
H_2O	3.0×10^{-5}
CO	2.0×10^{-5}
OCS	5.0×10^{-6}
S_2	7.5×10^{-7}
HCl	5.0×10^{-7}
S_n ($3 \leq n \leq 8$)	3.3×10^{-7}
NO	5.5×10^{-9}
H_2	3.0×10^{-9}
H_2S	1.0×10^{-9}
SO	3.0×10^{-11}
$ClSO_2$	3.0×10^{-11}
SO_2Cl_2	1.0×10^{-11}
HS	8.0×10^{-13}
SNO	1.0×10^{-13}
SCl	6.7×10^{-15}
HSCl	2.8×10^{-15}
Cl_2	1.0×10^{-16}
S	7.5×10^{-17}
H	7.3×10^{-19}
OH	7.3×10^{-19}

Supplementary Table 3. Observational constraints on atmospheric concentrations

Species	Atmospheric Height	Mixing Ratio	Reference
CO	12 km	2×10^{-5}	[49]
	22 km	2×10^{-5}	[49]
	25 km	2.5×10^{-5}	[49]
	36 km	3×10^{-5}	[96]
	40 km	3×10^{-5}	[49]
	45 km	3.5×10^{-5}	[49]
OCS	30 km	1.1×10^{-5}	[49]
	33 km	3×10^{-6}	[96]
	36 km	1.1×10^{-6}	[49]
	64 km	1.4×10^{-8}	[97]
	70 km	2×10^{-9}	[97]
SO_2	35 km	1.5×10^{-4}	[96]
	75 km	5×10^{-8}	[98], Average from several observations
	90 km	1×10^{-7}	[98], Average from several observations
	100 km	1×10^{-7}	[98], Average from several observations
H_2O	35 km	3.2×10^{-5}	[96]
	70 km – 100 km	1×10^{-6}	[99], Constant between these heights
H_2S	70 km	$< 2.3 \times 10^{-8}$	[97], Upper Limit
HCl	65 km – 95 km	2×10^{-7}	[99], Constant between these heights
S_3	6.5 km	1.1×10^{-11}	[49], Heights are approximate
	15 km	1.8×10^{-11}	[49], Heights are approximate
SO	90 km	2×10^{-8}	[98], Average from several observations
	100 km	1×10^{-7}	[98], Average from several observations
PH_3	60 km	1×10^{-8}	This work

Supplementary References:

63   Counselman, C. C., Gourevitch, S. A., King, R. W., Loriot, G. B. & Ginsberg, E. S. Zonal and meridional circulation of the lower atmosphere of Venus determined by radio interferometry. *Journal of Geophysical Research: Space Physics* **85**, 8026-8030 (1980).

64   Sánchez-Lavega, A. *et al.* Variable winds on Venus mapped in three dimensions. *Geophysical Research Letters* **35** (2008).

65   Cardelino, B. H. *et al.* Semiclassical calculation of reaction rate constants for homolytical dissociation reactions of interest in organometallic vapor-phase epitaxy (OMVPE). *The Journal of Physical Chemistry A* **107**, 3708-3718 (2003).

66   Davidson, D. F., Kohse-Höinghaus, K., Chang, A. Y. & Hanson, R. K. A pyrolysis mechanism for ammonia. *International journal of chemical kinetics* **22**, 513-535 (1990).

67   Kaye, J. A. & Strobel, D. F. Phosphine photochemistry in the atmosphere of Saturn. *Icarus* **59**, 314-335 (1984).

68   Bolshova, T. A. & Korobeinichev, O. P. Promotion and inhibition of a hydrogen-oxygen flame by the addition of trimethyl phosphate. *Combustion, Explosion and Shock Waves* **42**, 493-502 (2006).

69   Rock, P. A. *Chemical thermodynamics: principles and applications*. (The Macmillan Company, 1969).

70   Greiner, W., Neise, L. & Stöcker, H. *Thermodynamics and statistical mechanics*. (Springer Science & Business Media, 2012).

71   Perrot, P. *A to Z of Thermodynamics*. (Oxford University Press on Demand, 1998).

72   Andreichikov, B. M. Chemistry of Small Components of Upper Shells of Venus. *Lunar and Planetary Science Conference* **29**, 1003 (1998).

73   Marcq, E., Mills, F. P., Parkinson, C. D. & Vandaele, A. C. Composition and chemistry of the neutral atmosphere of Venus. *Space Science Reviews* **214**, 10 (2018).

74   Oyama, V. *et al.* Pioneer Venus gas chromatography of the lower atmosphere of Venus. *Journal of Geophysical Research: Space Physics* **85**, 7891-7902 (1980).

75   Taylor, F. W. & Hunten, D. M. in *Encyclopedia of the Solar System*, 305-322 (Elsevier, 2014).

76   Vandaele, A. C. *et al.* Sulfur dioxide in the Venus atmosphere: I. Vertical distribution and variability. *Icarus* **295**, 16-33 (2017).

77   Smrekar, S. E., Stofan, E. R. & Mueller, N. in *Encyclopedia of the Solar System*, p323-341 (Elsevier, 2014).

78   Taylor, F. W., Svedhem, H. & Head, J. W. Venus: the atmosphere, climate, surface, interior and near-space environment of an Earth-like planet. *Space Science Reviews* **214**, 35 (2018).

79   Holland, H. D. *The chemical evolution of the atmosphere and oceans*. (Princeton University Press, 1984).

80   Glindemann, D., de Graaf, R. M. & Schwartz, A. W. Chemical Reduction of Phosphate on the Primitive Earth. *Origins of life and evolution of the biosphere* **29**, 555-561, doi:10.1023/A:1006622900660 (1999).

81   Glindemann, D., Edwards, M. & Schrems, O. Phosphine and methylphosphine production by simulated lightning—a study for the volatile phosphorus cycle and cloud formation in the earth atmosphere. *Atmospheric Environment* **38**, 6867-6874, doi:10.1016/j.atmosenv.2004.09.002 (2004).

82   Peucker-Ehrenbrink, B. Accretion of extraterrestrial matter during the last 80 million years and its effect on the marine osmium isotope record. *Geochimica et Cosmochimica Acta* **60**, 3187-3196, doi:10.1016/0016-7037(96)00161-5 (1996).

83   Emiliani, C. *Planet Earth: Cosmology, Geology, and the Evolution of Life and Environment*. (Cambridge University Press, 1992).

84   Geist, V., Wagner, G., Nolze, G. & Moretzki, O. Investigations of the meteoritic mineral (Fe,Ni)3P. *Crystal Research and Technology* **40**, 52-64, doi:10.1002/crat.200410307 (2005).

85   Cockell, C. S. Life on Venus. *Planetary and Space Science* **47**, 1487-1501 (1999).

86   Grinspoon, D. H. *Venus revealed: a new look below the clouds of our mysterious twin planet* (1997).

87   Schulze-Makuch, D., Grinspoon, D. H., Abbas, O., Irwin, L. N. & Bullock, M. A. A sulfur-based survival strategy for putative phototrophic life in the Venusian atmosphere. *Astrobiology* **4**, 11-18 (2004).

88   Wu, Z. *et al.* The near-UV absorber OSSO and its isomers. *Chemical Communications* **54**, 4517-4520, doi:10.1039/C8CC00999F (2018).

89   Bains, W., Petkowski, J. J., Sousa-Silva, C. & Seager, S. Trivalent Phosphorus and Phosphines as Components of Biochemistry in Anoxic Environments. *Astrobiology* **19**, 885-902, doi:10.1089/ast.2018.1958 (2019).

90   Way, M. J. & Del Genio, A. in *EPSC-DPS Joint Meeting* **13,** 1846 (Geneva, Switzerland, 2019).

91   Way, M. J. *et al.* Was Venus the first habitable world of our solar system? *Geophysical Research Letters* **43**, 8376-8383 (2016).

92   Phillips, R. J. *et al.* Impact craters and Venus resurfacing history. *Journal of Geophysical Research: Planets* **97**, 15923-15948 (1992).

93   Gillmann, C. & Tackley, P. Atmosphere/mantle coupling and feedbacks on Venus. *Journal of Geophysical Research: Planets* **119**, 1189-1217 (2014).

94   Amato, P. *et al.* Metatranscriptomic exploration of microbial functioning in clouds. *Scientific Reports* **9** (2019).

95   Bryan, N. C., Christner, B. C., Guzik, T. G., Granger, D. J. & Stewart, M. F. Abundance and survival of microbial aerosols in the troposphere and stratosphere. *The ISME journal*, 1-11 (2019).

96   Marcq, E. *et al.* A latitudinal survey of CO, OCS, H2O, and SO2 in the lower atmosphere of Venus: Spectroscopic studies using VIRTIS-H. In *Journal of Geophysical Research: Planets* **113** (2008).

97   Krasnopolsky, V. A. High-resolution spectroscopy of Venus: Detection of OCS, upper limit to H2S, and latitudinal variations of CO and HF in the upper cloud layer. *Icarus* **197**, 377-385 (2008).

98   Belyaev, D. A. *et al.* Vertical profiling of SO2 and SO above Venus' clouds by SPICAV/SOIR solar occultations. *Icarus* **217**, 740-751 (2012).

99   Bertaux, J.L. *et al.* A warm layer in Venus' cryosphere and high-altitude measurements of HF, HCl, H2O and HDO. *Nature* **450**, 646-649 (2007).